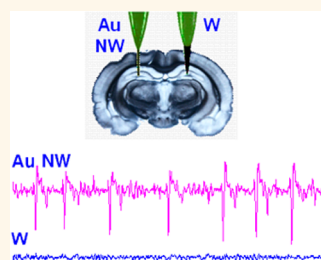


# Subcellular Neural Probes from Single-Crystal Gold Nanowires

Mijeong Kang,<sup>†</sup> Seungmoon Jung,<sup>‡</sup> Huanan Zhang,<sup>‡</sup> Taejoon Kang,<sup>||</sup> Hosuk Kang,<sup>†</sup> Youngdong Yoo,<sup>†</sup> Jin-Pyo Hong,<sup>#</sup> Jae-Pyung Ahn,<sup>⊗</sup> Juhyoun Kwak,<sup>†</sup> Daejong Jeon,<sup>‡,\*</sup> Nicholas A. Kotov,<sup>‡,\*</sup> and Bongsoo Kim<sup>†,\*</sup>

<sup>†</sup>Department of Chemistry and <sup>‡</sup>Department of Bio and Brain Engineering, KAIST, Daejeon 305-701, Korea, <sup>‡</sup>Department of Chemical Engineering, Biointerfaces Institute, University of Michigan, Ann Arbor, Michigan 48109, United States, <sup>||</sup>BioNanotechnology Research Center and BioNano Health Guard Research Center, KRIBB, Daejeon 305-806, Korea, <sup>#</sup>Department of Psychiatry, University of Ulsan College of Medicine, Asan Medical Center, Seoul 138-736, Korea, and <sup>⊗</sup>Nano Analysis Center, KIST, Seoul 130-650, Korea

**ABSTRACT** Size reduction of neural electrodes is essential for improving the functionality of neuroprosthetic devices, developing potent therapies for neurological and neurodegenerative diseases, and long-term brain–computer interfaces. Typical neural electrodes are micromanufactured devices with dimensions ranging from tens to hundreds of micrometers. Their further miniaturization is necessary to reduce local tissue damage and chronic immunological reactions of the brain. Here we report the neural electrode with subcellular dimensions based on single-crystalline gold nanowires (NWs) with a diameter of  $\sim 100$  nm. Unique mechanical and electrical properties of defect-free gold NWs enabled their implantation and recording of single neuron-activities in a live mouse brain despite a  $\sim 50\times$  reduction of the size compared to the closest analogues. Reduction of electrode dimensions enabled recording of neural activity with improved spatial resolution and differentiation of brain activity in response to different social situations for mice. The successful localization of the epileptic seizure center was also achieved using a multielectrode probe as a demonstration of the diagnostics potential of NW electrodes. This study demonstrated the realism of single-neuron recording using subcellular-sized electrodes that may be considered a pivotal point for use in diverse studies of chronic brain diseases.



**KEYWORDS:** gold nanowire · nanoelectrode · neural implants · neuroprosthetics · brain–machine interface · neurodegenerative disease · epilepsy · subcellular-sized implants · BRAIN initiative · single-neuron detection · electrode miniaturization · long-term neural recordings · paralysis

Recording neural electrodes represent the key elements in brain–machine interface and therapies for debilitating conditions such as paralysis. Long-term neural recordings are also much needed for a better understanding of neurodegenerative diseases, which currently affect more than 50 million people around the world, representing one of our most significant medical challenges. Several research groups demonstrated that reducing the size of implants to dimensions comparable to or smaller than those of neural cells' soma is essential for reducing inflammation around electrodes. Inflammatory reactions of the brain and subsequent glial encapsulation severely restricts the long-term functionalities of the electrodes.<sup>1–3</sup> Previous studies also highlighted the role of stiffness mismatch between the brain tissue and brain implants in activation of resident immune cells,<sup>4,5</sup> which stimulated the development of electrodes based on soft polymers<sup>6–8</sup> and composites.<sup>9</sup> Miniaturization

of the implants are expected to effectively reduce both acute/chronic trauma and improve their mechanical compliance with brain tissues.<sup>9</sup> As such, the implants with a diameter of *ca.* 10  $\mu\text{m}$  have shown to substantially reduce glial encapsulation.<sup>10</sup> The smallest known implants capable of recording neuronal activity had diameters of *ca.* 8  $\mu\text{m}$ , and their ability to record single neuronal spikes for 5 weeks was reported.<sup>11</sup> It is expected that the brain electrode implants necessary for detailed diagnostics and successful treatment of the diseases mentioned above will need to have several hundred individual electrodes assembled in arrays. High-density arrays of even the smallest recording electrodes used now can cause serious chronic tissue damage for long-term implantation, which translates to a requirement for further reduction of individual electrodes' dimensions.

The goal of this study was to investigate the possibility of miniaturization of implantable recording electrodes to submicrometer

\* Address correspondence to clark@kaist.ac.kr (D. Jeon); kotov@umich.edu (N. A. Kotov); bongsoo@kaist.ac.kr (B. Kim).

Received for review May 5, 2014 and accepted July 25, 2014.

Published online August 12, 2014  
10.1021/nn5024522

© 2014 American Chemical Society

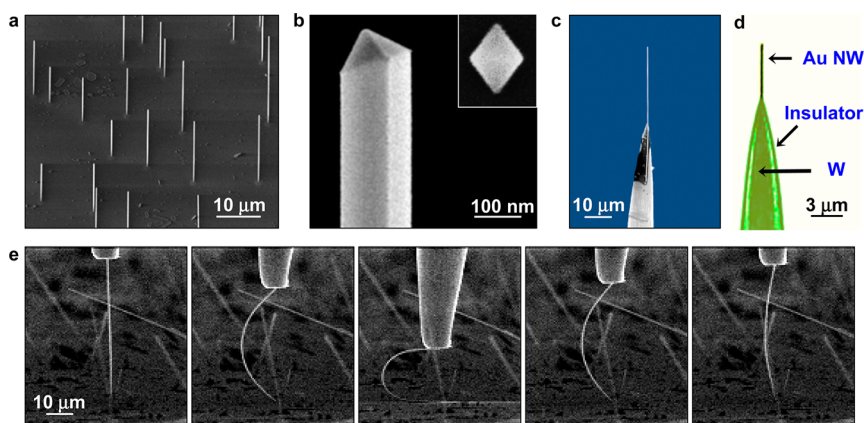


**Figure 1.** Characterization of Au NWs and neural probes from them. (a) Tilted 45° SEM image of vertically grown Au NWs on a *c*-cut sapphire substrate. (b) SEM image of a Au NW at higher magnification. The inset shows a top-view SEM image of a Au seed having a diamond-shape cross-section from which a Au NW is grown vertically maintaining its cross-section. (c) SEM image of a combined Au NW-tungsten-tip electrode. The image was obtained before insulation for a clear SEM image. (d) Optical image of a combined Au NW-tungsten-tip electrode. The tungsten (W) part was completely insulated with nail varnish (green-colored region). (e) SEM images captured during U-shape bending and complete recovery of a Au NW, showing superflexibility of a Au NW. The Au NW was pushed against a solid surface and then retracted back.

dimensions while also minimizing cell damage. Here we show that the recording neural electrodes can be made from single Au nanowires (NWs) with diameters of  $\sim 100$  nm based on our recent synthetic findings.<sup>12</sup> Despite their very small diameter, the near perfect crystallinity of the Au NWs enables them to maintain high mechanical strength and high electrical conductivity, which are highly desirable properties for recording implants.<sup>13,14</sup> Among the development of other approaches based on new materials,<sup>8</sup> successful implantation and recording of neural signals with these NWs would indicate that they represent a new milestone in miniaturization of brain implants; implantable devices of this size can greatly reduce the insertion trauma, improve mechanical compliance with brain tissue, and minimize the mechanoactivation of the resident immune cells.<sup>4</sup> High biocompatibility of gold and its long-term use as various implants also bode well for their use as neural implants.

We manufactured, implanted, and tested neural electrodes made from single-crystalline Au NWs and demonstrated their ability to record single neuronal spike trains in the brain, which validated the concept of functional recording electrodes with subcellular dimensions. The signal-to-noise (S/N) ratios of these recordings were substantially higher than those of conventional tungsten electrodes. This enabled us to detect variations in neural activity. Moreover, we were able to accomplish such measurements in a freely moving mouse and investigate mouse brain response depending on the social situation. In addition, pairs of Au NW electrodes implanted in the mouse brains were able to locate an epileptic seizure center with high spatial resolution.

Au NWs were vertically grown on a *c*-cut sapphire substrate by the vapor transport method.<sup>12</sup> They are defect-free single crystals (Figure S1, Supporting Information) with (111) surfaces on the sides and have

diameters in the range 30–150 nm and lengths up to  $\sim 100$   $\mu\text{m}$  (Figure 1a,b). We attached single Au NWs onto sharply etched tungsten tips using a conductive adhesive and a nanomanipulator (Figure 1c and Figure S2, Supporting Information). The tungsten part of the electrode was then insulated by dipping it into a nail varnish solution.<sup>15</sup> Importantly, the Au NWs display atomically smooth surfaces and a chisel-shaped tip (Figure 1b), which are significant advantages for implantation; the NWs penetrate into brain tissue with minimum compression damage and tearing of tissue.<sup>16</sup> The tungsten part of the NW electrode follows the path made by the Au NW and imparts significantly less acute damage than a tungsten tip without the Au NW during the implantation of an electrode.

A cyclic voltammogram (CV) obtained from one NW electrode confirms its single-crystalline nature<sup>17–19</sup> (Figure 2), while the sigmoidal shape of the steady-state CV indicates that mass transport toward the electrode surfaces occurs *via* fast convergent diffusion, as is predicted for nanoscale electrodes (Figure 2).<sup>20–22</sup> All electrochemical measurements were performed by using a potentiostat with a home-built three-electrode cell under optical microscope (Figure S3). A CV obtained in a 50 mM  $\text{H}_2\text{SO}_4$  solution revealed sharp peaks at 0.89 and 0.40 V (Figure 2a), associated with oxidation and reduction of a Au(111) surface.<sup>17</sup> No peaks related to the electrochemical reactions of tungsten were found, indicating that the tungsten part was completely insulated. We also measured the underpotential deposition (UPD) of copper (Cu) on a Au NW electrode as additional proof of its crystallinity (Figure 2b). The sharp reduction and oxidation CV peaks at  $-0.16$  V represent the deposition and dissolution of a Cu monolayer on Au(111) surfaces of a Au NW electrode. These well-defined Cu UPD peaks confirm that our Au NW electrode is single-crystalline with

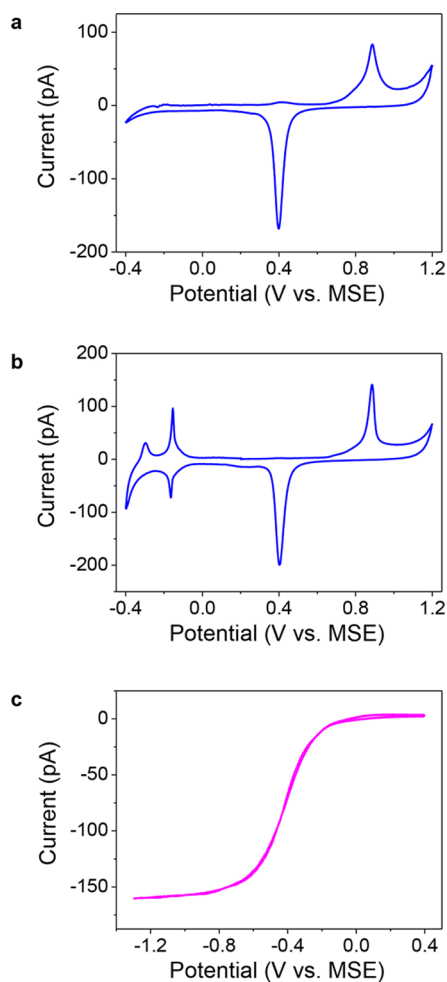


**Figure 2.** Electrochemical properties of Au NWs. (a) CV of a Au NW electrode in 50 mM H<sub>2</sub>SO<sub>4</sub> obtained at a scan rate of 50 mV/s. (b) CV of a Au NW electrode in a 5 mM CuSO<sub>4</sub>/50 mM H<sub>2</sub>SO<sub>4</sub> solution at a scan rate of 50 mV/s. The UPD (underpotential deposition) of Cu on a well-defined Au(111) surface of a Au NW electrode is observed at  $-0.16$  V. (c) CV of a Au NW electrode in a 20 mM K<sub>3</sub>Fe(CN)<sub>6</sub> solution without supporting electrolyte at a scan rate of 200 mV/s. Steady-state voltammetric response should be noted.

atomically flat surfaces.<sup>18,19</sup> The sigmoidal-shaped steady-state CVs of a Au NW electrode obtained in a 20 mM K<sub>3</sub>Fe(CN)<sub>6</sub> aqueous solution demonstrated that mass transport toward the electrode surface occurred fast *via* convergent diffusion, as predicted for very small nanoscale electrodes (Figure 2c).<sup>20–22</sup> The observed electrochemical characteristics of our Au NW electrode demonstrate that it performs as a high-quality electrode with appropriate electrical interfacial conditions for neuroprosthetic devices despite their nanoscale size.

A single Au NW showed a resistance of 52  $\Omega$  and resistivity of  $2.08 \times 10^{-8}$   $\Omega\text{m}$  (Figure S4a, Supporting Information), which is slightly smaller than the bulk resistivity of a perfect gold lattice of  $2.21 \times 10^{-8}$   $\Omega\text{m}$ .<sup>22</sup> The average impedance of seven Au NW electrodes measured at a biologically relevant frequency of 1 kHz was 5.6 M $\Omega$  (Figure S4c, Supporting Information). While

the surface area of the as-prepared Au NW electrodes was 10 times smaller than that of microscale tungsten electrodes used in control experiments (Figure S5), the impedance of the former was only 3 times higher than that of the latter. We attribute this to the high electric conductivity of Au NWs.<sup>14</sup>

Finally, Au NWs show excellent flexibility, as illustrated in Figure 1e, where a Au NW is bent into a U-shape and then completely recovered. Furthermore, they show a high yield strength of 1.54 GPa, 10 times the value of bulk gold.<sup>13</sup> Such unique mechanical characteristics originate from their defect-free single-crystalline nature.<sup>23</sup> This mechanical characteristic would help a Au NW to be flexibly inserted into the neural tissue and keep its linear geometry in the tissue. We observed that a Au NW electrode was easily inserted into transparent agarose gel, the mechanical behavior of which is similar to that of a neural tissue and maintained its straight form in the gel (Figure S6a,b, Movie S1, Movie S2, Supporting Information). In addition, we found that a Au NW can also pierce a single neuron in a brain slice (Figure S6c,d, Supporting Information).

The possibility of insertion of single NWs into the brain similar to other implantable electrodes can also be established from the calculations of their compliance with the brain tissue using the nanoscale mechanics analysis developed for composite electrodes in a previous publication.<sup>9</sup> As the electrodes are getting even smaller, it will be essential to establish a theoretical toolbox enabling one to evaluate the ability of the electrode to penetrate brain tissue prior to the experiment. It can be done considering the critical buckling pressure of the electrodes,  $P_{\text{crit}}$ . When the electrode is considered as a nanoscale beam,  $P_{\text{crit}}$  needs to be greater than the rupture strength of the brain tissue,  $P_{\text{brain}}$  (about 3 kPa), so that the electrode can be inserted into the tissue. For Au NW electrodes having a cross-sectional square of 100 nm side length and 100  $\mu\text{m}$  in length,  $P_{\text{crit}}$  is calculated to be 16 kPa.<sup>9</sup> This is much greater than  $P_{\text{brain}} = 3$  kPa and is therefore sufficient for successful insertion. These calculations also indicate that from the perspective of mechanics and implantation by insertion the diameter of the electrode can be further reduced if electrical properties of the electrode and its interface with cells make registration of neural signals possible.

So, the sum of unique material properties of Au NWs makes their utilization as implantable electrodes possible. We measured the neural signals in the brain of a freely moving mouse using two Au NW electrodes implanted 1 mm apart in the hippocampus CA1 region of a mouse brain (Figure 3a). Neural signals were recorded in 60 s intervals for the duration of 7 days subsequent to the surgery (Figure 3b,c). For comparison, we also recorded neural signals using two tungsten electrodes without Au NW tips, implanted following an identical protocol and pair arrangement. Figure S5

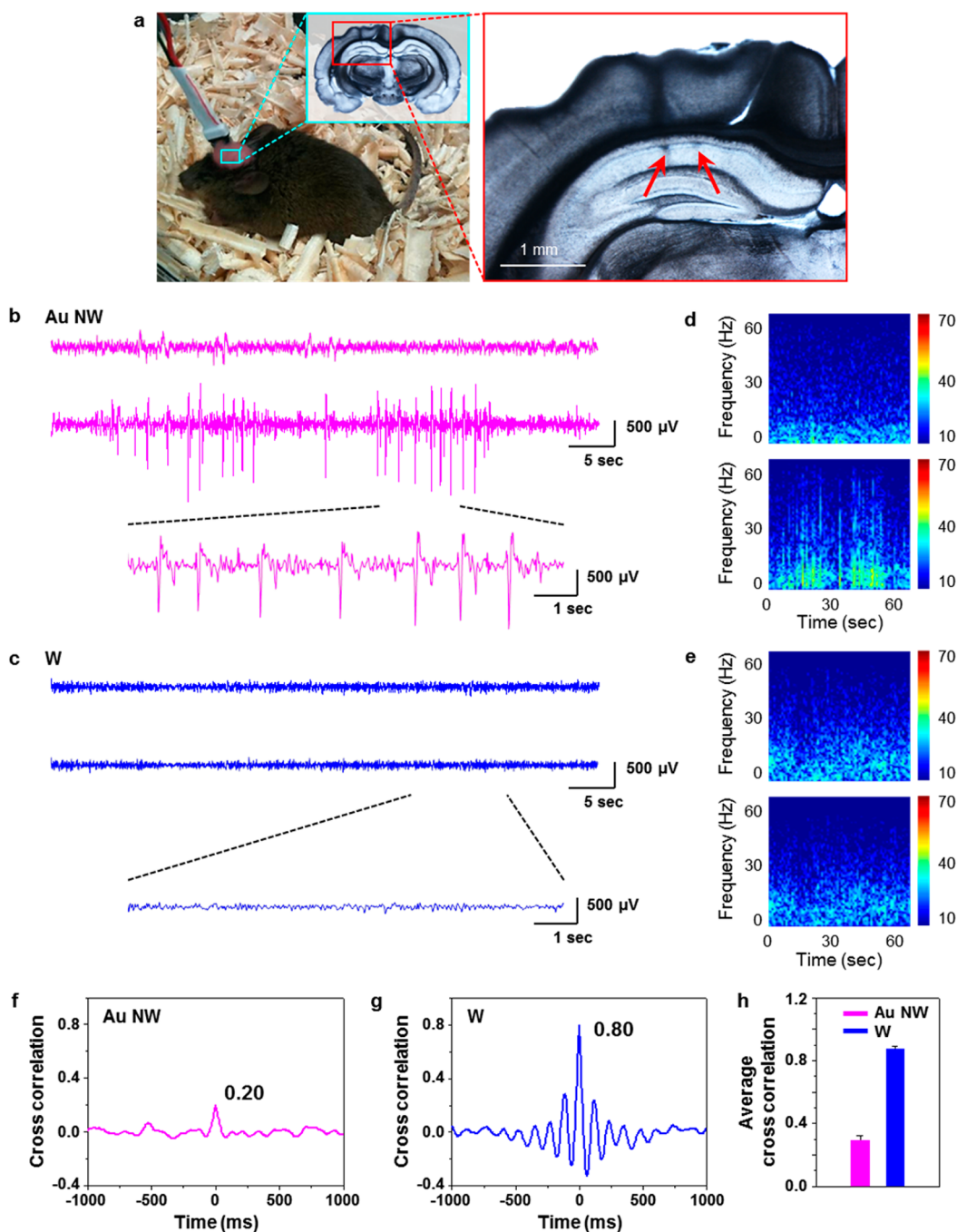


**Figure 3.** Neural signals recorded by Au NW and tungsten electrodes. (a) Photograph of a mouse from which we obtained neural signals using recording electrodes (left). Post-mortem histology of the recording regions and a coronal brain slice show the positions (arrows) of electrodes in the hippocampus (right). (b) Representative traces of neural signals recorded by two Au NW electrodes implanted within 1 mm apart in the hippocampal CA1 region of a living mouse brain for 60 s (top, middle). Selected section of the middle trace for 10 s is enlarged at the bottom. Characteristic neural spike signals were distinctly recorded. The two Au NW electrodes recorded quite different neural signals, providing independent information on local neural activity. (c) Representative traces of neural signals recorded by two tungsten electrodes implanted within 1 mm apart in the CA1 of a living mouse brain for 60 s (top, middle). Selected section of the middle trace for 10 s is enlarged at the bottom. Tungsten electrodes recorded highly correlated neural signals without distinct spike signals. (d, e) Colored power spectra of the traces shown in (b) and (c), respectively. (f, g) Cross-correlation analyses of the traces shown in (b) and (c), respectively. (h) Averaged first-peak values of the correlation analyses of neural signals recorded by Au NW ( $n = 6$ ) and tungsten ( $n = 8$ ) electrodes. There was a significant difference in the peak values between the two electrodes. The error bars represent standard mean deviation. \* $p < 0.05$ , Mann–Whitney U test.

shows optical images of the employed Au NW electrode (A) and the tungsten (B) electrode. The control tungsten implants had a tapered geometry with 1  $\mu$ m diameter in

the middle part of the electrode and were identical to the shank electrodes to which the Au NWs were attached.

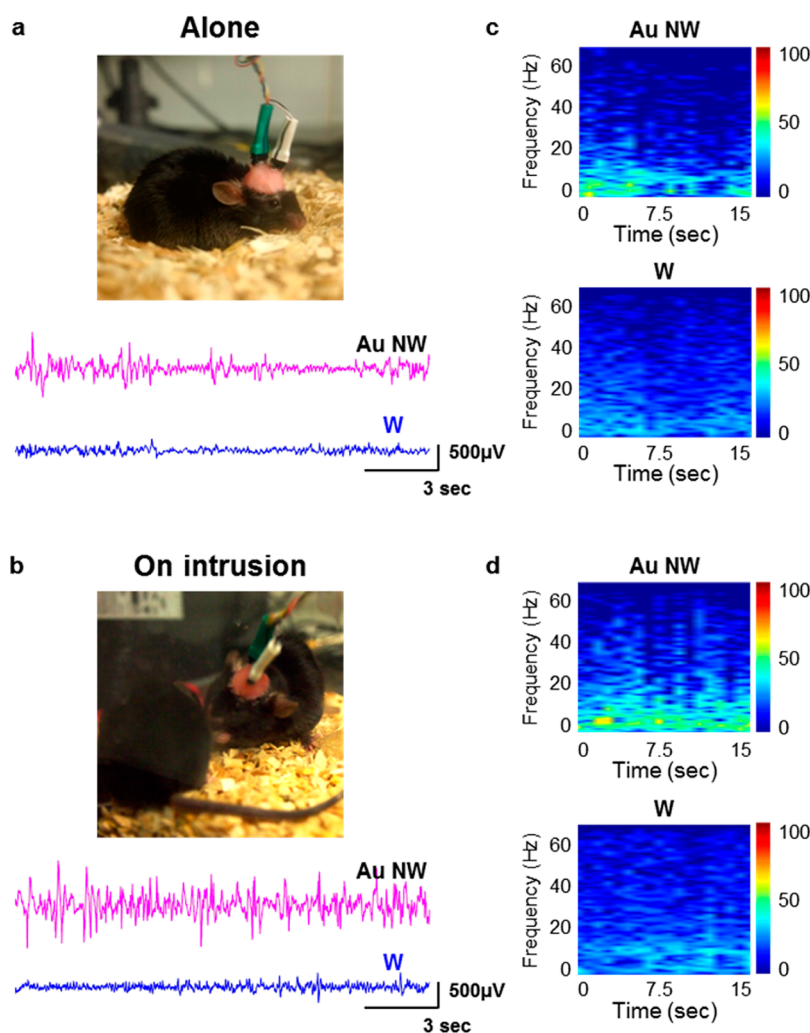


**Figure 4.** Neural response to different social situations: the intrusion by an unfamiliar mouse. (a) Representative traces of neural signals from Au NW (upper) and tungsten (bottom) electrodes implanted in the hippocampal CA1 region of a mouse moving alone in a confined space as shown in the photograph. (b) Representative traces of neural signals from Au NW (upper) and tungsten (bottom) electrodes implanted in CA1 of a mouse on intrusion by an unfamiliar mouse as shown in the photograph. Only the Au NW electrode shows spike signals upon the intrusion, indicating enhanced neural activity. (c, d) Power spectra of the traces shown in (a) and (b), respectively.

A characteristic train of neural spikes was observed for the Au NW electrodes (Figure 3b,d, Figure S7) and was barely visible for the two tungsten electrodes (Figure 3c,e, Figure S8), although both electrodes displayed similar baseline oscillation. Distinct neural spikes, observed in less than 1 h after the surgery, which was indicative of minimal neural damage around the Au NW. The spikes maintained a high S/N ratio for the entire period of the experiment (7 days), which was limited only by current animal care protocols. We noticed the neural signals measured from two Au NW electrodes simultaneously implanted in the mouse brain as described above were different and investigated their interdependence by cross-correlation analysis and in comparison with tungsten electrodes (Figure 3f–h). Averaged first-peak values of the neural signals from Au NW ( $n = 6$ ) and tungsten ( $n = 8$ ) electrodes were 0.28 and 0.88, respectively (Figure 3h). There was a significant difference in

correlation values of the two electrodes ( $p < 0.05$ ). This result confirmed the expectations that Au NW electrodes could provide higher spatial resolution than the tungsten microscale implants.

These *in vivo* observations and high-quality recordings of local neural activity were conducive to the possibility of detailed mapping of brain activity needed for fundamental studies of brain functions, diagnostics of many diseases, and brain–machine interface.<sup>24</sup> Therefore, we decided to record brain neural signals under different conditions for mice. One set of conditions modeled social interaction, and another set of conditions was a simulated disease state.

In the first series of experiments, we exposed a mouse with Au NW implants to a situation when an unfamiliar mouse intruded into its space. Figure 4a shows neural signals recorded from a mouse moving alone, and Figure 4b contrasts the previous data with signals observed after the intrusion of another animal.

We observed that the spike signals were remarkably enhanced after the intrusion, signifying a higher level of emotion or attention to the intruder and the correlated enhancement of brain activity. The corresponding higher power spectrum also displayed neural signals with greater intensity related to the excited status of a mouse (Figure 4c,d, upper). With the tungsten electrodes, the neural signals and corresponding higher power spectrum showed only subtle change after the intrusion (Figure 4c, d, bottom). Figures S9 and S10 show the alteration of total power intensity of neural signals during experiments and each trace of signals from both before and after social interaction with Au NW or tungsten electrodes.

In the second series of experiments, we replicated a case of epilepsy, one of the most common neurological diseases. It is characterized by seizure episodes, neurodegeneration, inflammation in the brain<sup>25,26</sup>, and is associated with greatly enhanced neural activity.<sup>27</sup> For the treatment of epilepsy, it is important to locate accurately a seizure focus that generates the epileptic spikes.<sup>28</sup> We implanted three Au NW electrodes separated by 1 mm from each other in the hippocampus CA1 region of a mouse brain and recorded the neural signals after injection of pilocarpine, a muscarinic acetylcholine receptor agonist frequently used as a seizure-inducing agent (Figure 5a).<sup>29</sup> The recordings were also performed using tungsten electrodes for comparison (Figure 5b). A signal from one Au NW electrode (the middle trace in Figure 5a) showed distinct early spike activities with higher amplitudes than signals from other Au NW electrodes, suggesting that it would be feasible to accurately locate a seizure focus with high spatial resolution using the Au NW electrodes, while it was nearly impossible with three larger tungsten electrodes. Figure S11 shows each trace from both Au NW and tungsten electrodes after pilocarpine injection and their cross-correlation among neural signals to compare spatial resolution.

The improved S/N ratio of acute neural signals obtained from the Au NW electrode is mainly attributed to minimized neural tissue damage around the electrode and size reduction of the recording site, limiting interference from the electrical activity of neighboring cells, temporal effects, and background potential.<sup>30</sup> To employ Au NW electrodes in chronic neural recording, it would be necessary to implement further studies such as the investigation of micromotion of a Au NW electrode within the brain and the subsequent tissue damage.

## METHODS

**Fabrication of Au NW Electrodes.** A conducting adhesive-coated tungsten tip mounted on a nanomanipulator approached a single Au NW on a sapphire substrate (Figure S2a) and picked it up by gentle manipulation (Figure S2b). The Au NW-attached

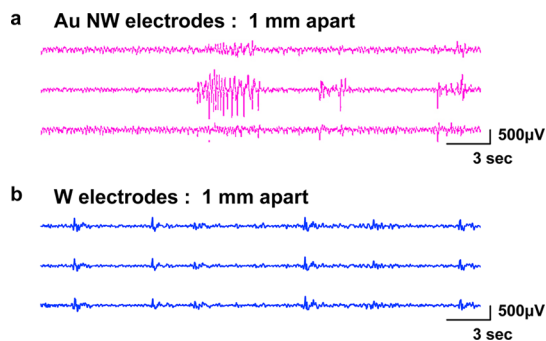


**Figure 5.** Detection of a seizure focus that generates the epileptic spikes. (a) Pilocarpine-induced seizure activities recorded by three Au NW electrodes separately implanted 1 mm apart in the CA1 of a living mouse brain. Seizure spike signals with high amplitudes are observed only in the middle trace. (b) Pilocarpine-induced seizure activities recorded by three tungsten electrodes separately implanted 1 mm apart in the CA1 of a living mouse brain. All neural signals are strongly correlated.

We found that single-crystalline Au NW electrodes with diameters as small as 100 nm were capable of reproducibly recording single-neuron activity. This capability of electrodes that are *ca.* 50 times smaller in diameter than previous implants is attributed to the special mechanical and electrical properties of single-crystal Au NWs. The subcellular dimension of the implants makes minimization of acute local trauma to brain tissue and high S/N ratio of recordings possible. The importance of such probes can be demonstrated by the acquired capabilities to distinguish the differences in neural activity depending on the actual real-time social situations and by registration and accurate spatial location of a seizure focus after the onset of an induced epileptic seizure, which will provide a pivotal point in the study and diagnostics of diseases. The submicrometer diameter of our electrodes makes recording neural activity with enhanced spatial precision better than fMRI<sup>24</sup> potentially possible, while mitigating the invasive nature of the implants. We anticipate that Au NW-based implants can be employed for diverse biological/medical/chemical studies based on local electrochemical processes<sup>31</sup> as well as for subsequent microfabrication in arrays. Further histological studies aimed at comparative tissue reactions to the implants and long-term recordings exceeding 12–24 months will be necessary for providing insight into their full clinical and research potential. In turn, this understanding will lead to greater use of the technology and possible new research breakthroughs.

tungsten tip was then insulated with nail varnish (Figure S2c). For the complete insulation, a middle area of the tungsten tip was immersed in nail varnish solution, moved back and forth several times, and dried in an ambient environment.

**Animals.** Young male C57BL/6 mice (22–25 g) were used for experiments. Mice were housed with a 12 h light/dark cycle and

*ad libitum* access to food and water. Animal care and handling were carried out according to the guidelines from the KAIST Institutional Animal Care and Use Committee (IACUC).

**In Vivo Neural Signal Measurements.** *In vivo* neural signals were recorded as described previously.<sup>29,32</sup> Animals were anesthetized by intraperitoneal injection of 1% ketamine (30 mg/kg) and xylazine hydrochloride (4 mg/kg), and the surgery was performed using a stereotaxic apparatus (Kopf Instruments). To obtain neural signals of mice, two Au NW (or two tungsten) electrodes were positioned in the right hemisphere at AP  $-1.8$ , L  $1.8$ , and DV  $1.5$  mm and AP  $-1.8$ , L  $0.8$ , and DV  $1.4$  mm (hippocampal CA1 regions) from the bregma with grounding over the cerebellum. In the experiment with pilocarpine, a third electrode was positioned in the right hemisphere at AP  $-2.5$ , L  $2.0$ , and DV  $1.4$  mm. Pilocarpine (330 mg/kg, intraperitoneal injection)-induced status epilepticus mice were also prepared by a previously reported method.<sup>29</sup> All electric activities were recorded after being amplified ( $1200\times$ ), band-pass-filtered from 0.1 to 70 Hz, and digitized at a 400 Hz sampling rate (AS 40) by using a digital electroencephalography system (Comet XL, Astro-Med, Inc., Warwick, RI, USA). To obtain colored power spectra, electroencephalography signals were filtered from 1 to 70 Hz. Colored power spectra were calculated and drawn with Fourier transformation of 2 s window sizes using Matlab.

**Social Interaction Experiment.** A single mouse (mouse 1) in the recording chamber cage was allowed to roam freely for 30 min (habituation). A novel and unfamiliar juvenile mouse (mouse 2) was introduced to the recording chamber of mouse 1 and allowed to roam freely for 1 min (test session). Electrical signals from mouse 1 during the first 15 s of the social interaction were analyzed.

**Electrochemical Measurements.** All electrochemical measurements were performed using a potentiostat (CHI 660D, CH Instruments) with a home-built three-electrode cell under optical microscope monitoring (Figure S3). To control the Au NW electrode precisely, we mounted the Au NW electrode on a three-dimensional piezoelectric stage (Sigma-Koki). A platinum wire and mercury/mercurous sulfate electrode (MSE, Hg/Hg<sub>2</sub>SO<sub>4</sub>) were used as counter and reference electrodes, respectively.

**Conflict of Interest:** The authors declare no competing financial interest.

**Supporting Information Available:** Experimental details including fabrication of Au NW electrodes, electrochemical measurements, electric properties of a Au NW electrode, investigation on the status of a Au NW electrode in brain tissue, and mechanical characteristics of the Au NW electrode. This material is available free of charge via the Internet at <http://pubs.acs.org>.

**Acknowledgment.** This work was supported by Korea Health 21 R&D grants (D.J.: H12C0035 and H12C1838) funded by the Ministry of Health and Welfare, through the NRF (D.J.: NRF-2014R1A2A2A01002608, B.K.: NRF-2012M3A2A1051686 and A121983), the KRIBB Initiative Research Program (T.K.), 1R21CA121841-01A2 (N.A.K.), Biointerfaces Institute (University of Michigan), and NSF EFRI-ODISSEI 1240264 and NSF CBET 1403777 projects. This research was also partially supported by the World Class University Program through the KOSEF (N.A.K., R33-2008-000-10021-0).

## REFERENCES AND NOTES

- Clark, J. J.; Sandberg, S. G.; Wanat, M. J.; Gan, J. O.; Horne, E. A.; Hart, A. S.; Akers, C. A.; Parker, J. G.; Willuhn, I.; Martinez, V.; *et al.* Chronic Microsensors for Longitudinal, Subsecond Dopamine Detection in Behaving Animals. *Nat. Methods* **2010**, *7*, 126–129.
- Skousen, J.; Merriam, S. M.; Srivannavith, O.; Perlin, G.; Wise, K. D.; Tresco, P. A. Reducing Surface Area while Maintaining Implant Penetrating Profile Lowers the Brain Foreign Body Response to Chronically Implanted Planar Silicon Microelectrode Arrays. *Prog. Brain Res.* **2011**, *194*, 167–180.
- Seymour, J. P.; Kipke, D. P. Neural Probe Design for Reduced Tissue Encapsulation. *Biomaterials* **2007**, *28*, 3594–3607.
- Gilletti, A.; Muthuswamy, J. Brain Micromotion around Implants in the Rodent Somatosensory Cortex. *J. Neural Eng.* **2006**, *3*, 189–195.
- Subbaroyan, J.; Martin, D. C.; Kipke, D. R. A Finite-Element Model of the Mechanical Effects of Implantable Microelectrodes in the Cerebral Cortex. *J. Neural Eng.* **2005**, *2*, 103–113.
- Grill, W. M. Signal Considerations for Chronically Implanted Electrodes for Brain Interfacing. In *Indwelling Neural Implants: Strategies for Contending with the in Vivo Environment*; Reichert, W. M., Ed.; CRC Press: Boca Raton, FL, 2008; pp 42–58.
- Cheung, K. C.; Renaud, P.; Tanila, H.; Djupsund, K. Flexible Polyimide Microelectrode Array for *in Vivo* Recordings and Current Source Density Analysis. *Biosens. Bioelectron.* **2007**, *22*, 1783–1790.
- Richardson-Burns, S. M.; Hendricks, J. L.; Foster, B.; Povlich, L. K.; Kim, D. H.; Martin, D. C. Polymerization of the Conducting Polymer Poly(3, 4-ethylenedioxythiophene) (PEDOT) around Living Neural Cells. *Biomaterials* **2007**, *28*, 1539–1552.
- Zhang, H.; Patel, P. R.; Xie, Z.; Swanson, S. D.; Wang, X.; Kotov, N. A. Tissue-Compliant Neural Implants from Microfabricated Carbon Nanotube Multilayer Composite. *ACS Nano* **2013**, *7*, 7619–7629.
- Biran, R.; Martin, D. C.; Tresco, P. A. Neuronal Cell Loss Accompanies the Brain Tissue Response to Chronically Implanted Silicon Microelectrode Arrays. *Exp. Neurol.* **2005**, *195*, 115–126.
- Kozai, T. D.; Langhals, N. B.; Patel, P. R.; Deng, X.; Zhang, H.; Smith, K. L.; Lahann, J.; Kotov, N. A.; Kipke, D. R. Ultrasmall Implantable Composite Microelectrodes with Bioactive Surfaces for Chronic Neural Interfaces. *Nat. Mater.* **2012**, *11*, 1065–1073.
- Yoo, Y.; Seo, K.; Han, S.; Varadwaj, K. S. K.; Kim, H. Y.; Ryu, J. H.; Lee, H. M.; Ahn, J. P.; Ihee, H.; Kim, B. Steering Epitaxial Alignment of Au, Pd, and AuPd Nanowire Arrays by Atom Flux Change. *Nano Lett.* **2010**, *10*, 432–438.
- Seo, J. H.; Yoo, Y.; Park, N. Y.; Yoon, S. W.; Lee, H.; Han, S.; Lee, S. W.; Seong, T. Y.; Lee, S. C.; Lee, K. B.; *et al.* Superplastic Deformation of Defect-Free Au Nanowires via Coherent Twin Propagation. *Nano Lett.* **2011**, *11*, 3499–3502.
- Critchley, K.; Khanal, B. P.; Gorzny, M. L.; Vigderman, L.; Evans, S. D.; Zubarev, E. R.; Kotov, N. A. Near-Bulk Conductivity of Gold Nanowires as Nanoscale Interconnects and the Role of Atomically Smooth Interface. *Adv. Mater.* **2010**, *22*, 2338–2342.
- Yoo, S. M.; Kang, M.; Kang, T.; Kim, D.; Lee, S. Y.; Kim, B. Electrotriggered, Spatioselective, Quantitative Gene Delivery into a Single Cell Nucleus by Au Nanowire Nanoinjector. *Nano Lett.* **2013**, *13*, 2431–2435.
- Edell, D. J.; Toi, V. V.; Mcneil, V. M.; Clark, L. D. Factors Influencing the Biocompatibility of Insertable Silicon Microshafts in Cerebral Cortex. *IEEE Trans. Biomed. Eng.* **1992**, *39*, 635–643.
- Kondo, T.; Morita, J.; Hanaoka, K.; Takakusagi, S.; Tamura, K.; Takahashi, M.; Mizuki, J.; Uosaki, K. Structure of Au(111) and Au(100) Single-Crystal Electrode Surfaces at Various Potentials in Sulfuric Acid Solution Determined by *in Situ* Surface X-Ray Scattering. *J. Phys. Chem. C* **2007**, *111*, 13197–13204.
- Herrero, E.; Buller, L. J.; Abruna, H. D. Underpotential Deposition at Single Crystal Surfaces of Au, Pt, Ag and Other Materials. *Chem. Rev.* **2001**, *101*, 1897–1930.
- Etsel, K. D.; Bickel, K. R.; Schuster, R. Heat Effects upon Electrochemical Copper Deposition on Polycrystalline Gold. *ChemPhysChem* **2010**, *11*, 1416–1424.
- Heller, I.; Kong, J.; Heering, H. A.; Williams, K. A.; Lemay, S. G.; Dekker, C. Individual Single-Walled Carbon Nanotubes as Nanoelectrodes for Electrochemistry. *Nano Lett.* **2005**, *5*, 137–142.
- Yum, K.; Cho, H. N.; Hu, J.; Yu, M. F. Individual Nanotube-Based Needle Nanoprobes for Electrochemical Studies in Picoliter Microenvironments. *ACS Nano* **2007**, *1*, 440–448.

22. Dawson, K.; Strutwolf, J.; Rodgers, K. P.; Herzog, G.; Arrigan, D. W. M.; Quinn, A. J.; O'Riordan, A. Single Nanoskived Nanowires for Electrochemical Applications. *Anal. Chem.* **2011**, *83*, 5535–5540.
23. Landman, U.; Luedtke, W. D.; Salisbury, B. E.; Whetten, R. L. Reversible Manipulations of Room Temperature Mechanical and Quantum Transport Properties in Nanowire Junctions. *Phys. Rev. Lett.* **1996**, *77*, 1362–1365.
24. Thulborn, K. R.; Chang, S. Y.; Shen, G. X.; Voyvodic, J. T. High-Resolution Echo-Planar fMRI of Human Visual Cortex at 3.0 T. *NMR Biomed.* **1997**, *10*, 183–190.
25. Fabene, P. F.; Mora, G. N.; Martinello, M.; Rossi, B.; Merigo, F.; Ottoboni, L.; Bach, S.; Angiari, S.; Benati, D.; Chakir, A.; *et al.* A Role for Leukocyte-Endothelial Adhesion Mechanisms in Epilepsy. *Nat. Med.* **2008**, *14*, 1377–1383.
26. Vezzani, A.; Granata, T. Brain Inflammation in Epilepsy: Experimental and Clinical Evidence. *Epilepsia* **2005**, *46*, 1724–1739.
27. Kim, D. H.; Viventi, J.; Amsden, J. J.; Xiao, J. L.; Vigeland, L.; Kim, Y. S.; Blanco, J. A.; Panilaitis, B.; Frechette, E. S.; Contreras, D.; *et al.* Dissolvable Films of Silk Fibroin for Ultrathin Conformal Bio-Integrated Electronics. *Nat. Mater.* **2010**, *9*, 511–517.
28. Kuzniecky, R.; Devinsky, O. Surgery Insight: Surgical Management of Epilepsy. *Nat. Clin. Pract. Neurol.* **2007**, *3*, 673–681.
29. Jeon, D.; Chu, K.; Lee, S. T.; Jung, K. H.; Kang, K. M.; Ban, J. J.; Kim, S.; Seo, J. S.; Won, C. H.; Kim, M.; *et al.* A Cell-Free Extract from Human Adipose Stem Cells Protects Mice against Epilepsy. *Epilepsia* **2011**, *52*, 1617–1626.
30. Kipke, D. R.; Pellinen, D. S.; Rousche, P. J. CNS Recording Electrodes and Techniques. In *Neuroprosthetics: Theory and Practice*; Horch, K. W., Dhillon, G. S., Eds.; World Scientific: Singapore, 2004; pp 773–776.
31. Kotov, N. A.; Winter, J. O.; Clements, I. P.; Jan, E.; Timko, B. P.; Campidelli, S.; Pathak, S.; Mazzatenta, A.; Lieber, C. M.; Prato, M.; *et al.* Nanomaterials for Neural Interfaces. *Adv. Mater.* **2009**, *21*, 1–35.
32. Jeon, D.; Kim, S.; Chetana, M.; Jo, D.; Ruley, H. E.; Lin, S. Y.; Rabah, D.; Kinet, J. P.; Shin, H. S. Observational Fear Learning Involves Affective Pain System and Cav 1.2 Ca<sup>2+</sup> Channels in ACC. *Nat. Neurosci.* **2010**, *13*, 482–490.